Aeronautical Research Institute, University of Tokyo
Report No. 356, May 1960

Symmetrical Buckling of Cylindrical Shells under External Pressure*

By

Megumi SUNAKAWA and Masuji UEMURA

Summary. The buckling phenomenon of cylindrical shells under external pressure was analyzed on the basis of the theory of finite deformation. Restricting our consideration to the case of boundary conditions; clamped straight edges and simply supported circumferential edges, the relations between the pressure and the deflection were obtained and the critical buckling pressures were discussed.

The main conclusions were as follows:

1. The "Durchschlag" phenomenon may take place more easily, if the values of $1/\lambda$, θ_0 and a/t are larger [$\lambda=(y_0/l)^2$, $y_0=a\theta_0$. See Fig. 2].
2. The buckling pressure are lower, if the values of $1/\lambda$, $1/\theta_0$ and a/t are larger.
3. The main characteristic for the case of cylindrical shell which differs from that of spherical shell lies in the fact that the buckling pressure has no minimum value against α ($\alpha=a\theta_0^2/t$).

The cases for other boundary conditions can be analyzed with the same process as described in this paper.

1. INTRODUCTION

The buckling phenomenon of the partial cylindrical shell or the curved plate under external pressure has had a great significance, for example, for the submarine structure, and lately some attention has been paid also to the buckling of the roof of hangar due to snow. To meet the need in such engineering problems, this buckling problem is here analyzed on the basis of the finite deformation theory.

We can find the papers concerning this buckling problem based on the infinitesimal deformation theory (linear theory). However, the classical critical buckling values of thin shells based on the linear theory are usually far higher than the experimental values, and this discrepancy between them has been explained from the nonlinear load–deflection curve or from the standpoint of potential energy on the basis of the finite deformation theory. Such an attempt was shown on the buckling of spherical shells under external pressure by one of the present authors [*1*]~[*4*]. This paper has thus a further aim to explain such a discrepancy between experiments and the theoretical values predicted by the linear theory. Since there enter more parameters for the case of the cylindrical shell than for the case of spherical shell, and the analytical results are too complicated to be expressed

* Read at the Special Meeting JSME, Oct. 29, 1959.

in a concrete form with satisfactory accuracy, then our consideration is restricted to the case of specific boundary conditions and particular symmetrical deformation for an example. But, the more general cases can be analyzed by the same process as described in this paper.

Nomenclatures and Symbols

a, l, t	average radius of curvature, axial half length and thickness of the undeformed cylindrical shell, respectively.
θ_0	center angle of the partial cylindrical shell.
p	radial pressure acting on the unit surface area of the cylindrical shell (positive when external pressure).
T_{11}, T_{22}	extensional forces per unit length of width after deformation in the x and y directions, respectively.
T_{12}	shearing force in the median surface after deformation.
T_{13}, T_{23}	shearing forces normal to the median surface after deformation.
G_1, G_2	bending mements after deformation about the x and y axes, respectively.
$L, N/a^2$	curvatures of the median surface after deformation about the x and y axes, respectively.
M/a	twist of the median surface after deformation.
κ_1, κ_2	curvature changes of the median surface about the x and y axes, respectively.
κ_{12}	change of twist of the median surface.
$\varepsilon_{11}, \varepsilon_{22}$	extensional strains in the median surface.
ε_{12}	shearing strain in the median surface.
B	flexural modulus of rigidity. $B \equiv Et^3/12(1-\nu^2)$
E	modulus of elasticity.
ν	Poisson's ratio.
x, y, z	coordinates in the axial, circumferential and radial directions in the median surface. (See Fig. 1)
u, v, w	displacement components on the median surface in the x, y and z directions, respectively, which are functions of x and y.

Suffixes "x" and "y" mean the differentiation with respect to x and y, respectively.

2. Equilibrium Equations and Compatibility Equation

The coordinates and the variables on the cylindrical shell are shown in Fig. 1 and Fig. 2. The origin of coordinates is taken at the midpoint of the median surface of the cylindrical shell. From the analysis based on the infinitesimal strain and the finite deformation [5], the equilibrium equations of cylindrical shell subjected to external pressure are given as follows :—

$$\frac{\partial T_{11}}{\partial x}+\frac{\partial T_{12}}{\partial y}-T_{13}L-T_{23}\frac{M}{a}=0, \tag{1-1}$$

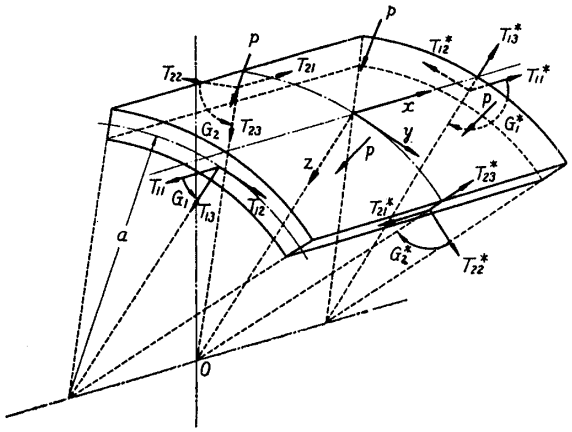

FIGURE 1.

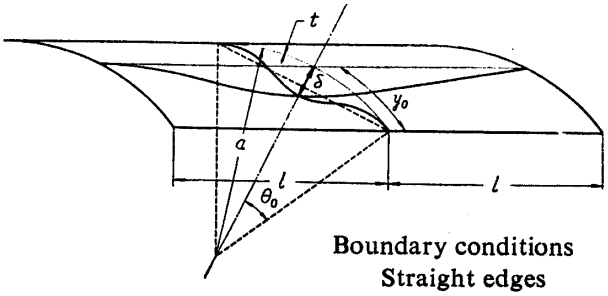

Boundary conditions
Straight edges : clamped
Circumferential edges : simply supported

FIGURE 2.

$$\frac{\partial T_{12}}{\partial x}+\frac{\partial T_{22}}{\partial y}-T_{13}\frac{M}{a}-T_{23}\frac{N}{a^2}=0, \tag{1-2}$$

$$\frac{\partial T_{13}}{\partial x}+\frac{\partial T_{23}}{\partial y}+T_{11}L+2T_{12}\frac{M}{a}+T_{22}\frac{N}{a^2}+p=0, \tag{1-3}$$

$$\frac{\partial H_1}{\partial x}+\frac{\partial G_2}{\partial y}+T_{23}=0, \tag{1-4}$$

$$\frac{\partial G_1}{\partial x}+\frac{\partial H_2}{\partial y}-T_{13}=0, \tag{1-5}$$

$$G_1=-B(\kappa_1+\nu\kappa_2), \tag{1-6}$$

$$G_2=B(\kappa_2+\nu\kappa_1), \tag{1-7}$$

$$H_1=-H_2=B(1-\nu)\kappa_{12}. \tag{1-8}$$

Curvatures L, M/a and N/a^2, curvature changes κ_1, κ_{12} and κ_2, and strain components ε_{11}, ε_{12} and ε_{22} can be expressed in terms of u, v and w and their derivatives, and their power functions on the basis of the finite deformation theory. For example, the strain components in the median surface can be written rigorously as follows:

$$\varepsilon_{11}=u_x+\frac{1}{2}(u_x^2+v_x^2+w_x^2),$$

$$\varepsilon_{12}=u_y+v_x+u_xu_y+v_x\left(v_y-\frac{w}{a}\right)+w_x\left(w_x+\frac{v}{a}\right),$$

$$\varepsilon_{22}=v_y-\frac{w}{a}+\frac{1}{2}\frac{w^2}{a^2}+\frac{1}{2}(u_y{}^2+v_y{}^2+w_y{}^2)-v_y\frac{w}{a}+w_y\frac{v}{a}+\frac{v^2}{a^2}.$$

Now, let δ be the maximum deflection at the midpoint of the partial cylindrical shell or the curved plate, and δ/y_0 and δ/l are assumed to be the infinitesimal quantities of the first order, and u and v to be smaller than w. In such a case where δ/t is not so large, the curvature changes and the curvatures of the median surface are given as follows by considering the first order terms only.

$$\left.\begin{aligned}\kappa_1&=w_{xx},\\ \kappa_{12}&=w_{xy},\\ \kappa_2&=w_{yy}+\frac{w}{a^2}.\end{aligned}\right\} \tag{2}$$

$$\left.\begin{aligned}L&=w_{xx},\\ \frac{M}{a}&=w_{xy},\\ \frac{N}{a^2}&=\frac{1}{a}+w_{yy}+\frac{w}{a^2}.\end{aligned}\right\} \tag{3}$$

In Eqs. (1–1) and (1–2), which are the equilibrium equations in the x and y directions, respectively, the 3rd and 4th terms are so small quantities compared with the 1st and 2nd terms that they can be neglected for the first approximation. Then this pair of equations can be satisfied by introducing the well-known Airy's stress function $\chi(x, y)$, defined by the relations

$$\left.\begin{aligned}\frac{T_{11}}{Et}&=\phi_1=\frac{\partial^2\chi}{\partial y^2},\\ \frac{T_{12}}{Et}&=\phi_{12}=-\frac{\partial^2\chi}{\partial x\partial y},\\ \frac{T_{22}}{Et}&=\phi_2=\frac{\partial^2\chi}{\partial x^2}.\end{aligned}\right\} \tag{4}$$

The strain components in the median surface can be also expressed as follows taking into account the quantities of the first order.

$$\left.\begin{aligned}\varepsilon_{11}&=\phi_1-\nu\phi_2=u_x+\frac{1}{2}w_x{}^2,\\ \varepsilon_{12}&=2(1+\nu)\phi_{12}=u_y+v_x+w_xw_y,\\ \varepsilon_{22}&=\phi_2-\nu\phi_1=v_y-\frac{w}{a}+\frac{1}{2}\left(\frac{w^2}{a^2}+w_y{}^2\right).\end{aligned}\right\} \tag{5}$$

Eliminating u and v from the three of Eqs. (5) and using χ in Eqs. (4), the following compatibility equation can be obtained.

$$\nabla^4\chi=w_{xy}^2-w_{xx}w_{yy}-\frac{w_{xx}}{a}+\frac{1}{a^2}(w_x{}^2+ww_{xx}). \tag{6}$$

The process of calculation is first to derive χ by solving Eq. (6) after substituting w that satisfies the boundary conditions into the right hand side of Eq. (6), and determining the integral constants so as to satisfy the boundary conditions on u and v, and then to obtain the pressure–deflection curves from the equilibrium equation in the z-direction of Eq. (1–3) to which the Galerkin's method is applied

after substituting Eqs. (1–4)∼(1–8).

According to this process, an example of analysis will be shown in the following section.

3. Approximate Solution of Equations

As an example of analysis, a curved plate will be considered where the straight edges are clamped and the circumferential edges are simply supported, and the deflection mode is symmetrical with respect to the center point. In this case, the boundary conditions are written as

$$\left.\begin{aligned} w=\frac{\partial^2 w}{\partial x^2}=0 \qquad & \text{on } x=\pm l, \\ w=\frac{\partial w}{\partial y}=0 \qquad & \text{on } y=\pm y_0, \end{aligned}\right\} \tag{7}$$

and the plausible function for w which satisfies these boundary conditions can be expressed as follows :

$$w=\delta_0(5-6x'^2+x'^4)(1-2y'^2+y'^4), \tag{8}$$

where

$$\delta_0=\frac{\delta}{5}, \qquad x'=\frac{x}{l}, \qquad y'=\frac{y}{y_0}. \tag{9}$$

Substituting Eq. (8) into Eq. (6), the compatibility eqation is expressed as

$$\begin{aligned} l^2\nabla^4\chi=4(1-y'^2)^2\{&3(-20\delta_1^2-5\delta_2^2+\delta_2)+30(6\delta_1^2+\delta_2^2)y'^2-15\delta_2^2y'^4 \\ &+3(44\delta_1^2+23\delta_2^2-\delta_2)x'^2+6(30\delta_1^2-23\delta_2^2)x'^2y'^2+69\delta_2^2x'^2y'^4 \\ &+3(-28\delta_1^2-15\delta_2^2)x'^4+6(-22\delta_1^2+15\delta_2^2)x'^4y'^2-45\delta_2^2x'^4y'^4 \\ &+(12\delta_1^2+7\delta_2^2)x'^6+14(2\delta_1^2-\delta_2^2)x'^6y'^2+7\delta_2^2x'^6y'^4\}, \end{aligned} \tag{10}$$

where

$$\delta_1=\frac{\delta_0}{y_0}, \qquad \delta_2=\frac{\delta_0}{a}. \tag{11}$$

The stress function χ is now assumed to be expressed in the following polynomial function.

$$l^2\chi=\sum_{\substack{m,n=0 \\ m+n\leq 9}}^{9} A_{mn}x'^{2m}y'^{2n} \tag{12}$$

The fifty-five unknown coefficients A_{mn}s in Eq. (12) can be determined exactly by solving simultaneously the following equations.

i) Substituting Eq. (12) into Eq. (10) and equalizing the corresponding coefficients of the terms $x'^{2m}y'^{2n}$ in both sides of the equation, the thirty-six equations on A_{mn}s are obtained as shown in Fig. 3, where the straight lines that connect three points mean the linear equations containing the three different A_{mn}s.

ii) The following equations can be derived from the first and the third of Eqs. (5).

$$\left.\begin{aligned} u_x&=\frac{T_{11}-\nu T_{22}}{Et}-\frac{1}{2}w_x{}^2, \\ v_y&=\frac{T_{22}-\nu T_{11}}{Et}+\frac{w}{a}-\frac{1}{2}\left(\frac{w^2}{a^2}+w_y{}^2\right). \end{aligned}\right\} \tag{13}$$

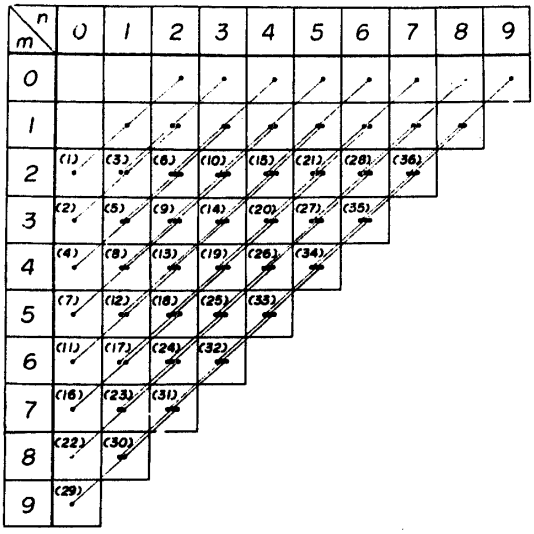

FIGURE 3.

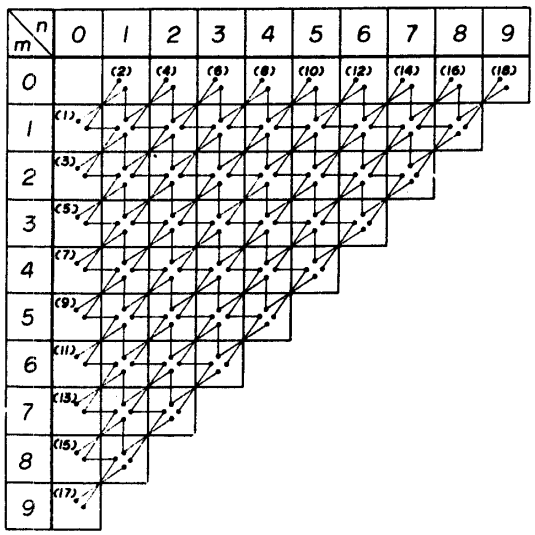

FIGURE 4.

Integrating Eqs. (13) with respect to x and y, respectively, and using the boundary conditions :

$$(u)_{x'=0,\pm1}=0, \qquad (v)_{y'=0,\pm1}=0, \tag{14}$$

then the eighteen equations on A_{mn}s can be obtained from the edge conditions as shown in Fig. 4 after determining the integral constants by $(u)_{x'=0}=0$ and $(v)_{y'=0}=0$.

iii) $$A_{00}=0. \tag{15}$$

All the coefficients A_{mn}s thus determined from the equations in i), ii) and iii) can be presented in the following form.

$$\frac{A_{mn}}{y_0^2}=(a_{mn}+b_{mn}\theta_0^2)\delta^2+c_{mn}a\theta_0^2\delta, \tag{16}$$

where a_{mn}s, b_{mn}s and c_{mn}s are the functions of $\lambda=y_0^2/l^2$ and Poisson's ratio ν. If ν is put equal to a constant such as 1/3, then a_{mn}s, b_{mn}s and c_{mn}s can be shown in the polynomial form of λ only as

$$a_{mn}=\sum_{i=-5}^{3}a_{mn,i}\lambda^i, \qquad b_{mn}=\sum_{i=-6}^{3}b_{mn,i}\lambda^i, \qquad c_{mn}=\sum_{i=-4}^{1}c_{mn,i}\lambda^i. \tag{17}$$

Now that the stress function has been determined in the manner described above, the Galerkin's method is applied to Eq. (1-3), that is, corresponding to the minimum principle of the potential energy, the following operation can be used to get the relation between the pressure and the deflection.

$$\int_{-y_0}^{y_0}\int_{-l}^{l}\left\{\frac{\partial T_{13}}{\partial x}+\frac{\partial T_{23}}{\partial y}+T_{11}w_{xx}+2T_{12}w_{xy}+T_{22}\left(\frac{1}{a}+w_{yy}+\frac{w}{a^2}\right)+p\right\}w\,dx\,dy=0, \tag{18}$$

where, T_{11}, T_{12} and T_{22} are given by Eqs. (4) and (12), and T_{13} and T_{23} are given by Eqs. (1-4)$\sim$(1-8) and (2).

As an example, the external pressure is assumed to be distributed as

$$p=p_0(1-y'^2). \tag{19}$$

Integrating Eq. (18) under the pressure distribution as Eq. (19), the relation between the pressure and the maximum deflection is finally expressed as follows:

$$\frac{a^2p_0}{Et^2}=\frac{1}{\alpha^2}\left\{f_1(\lambda)+f_2(\lambda)\theta_0^2+f_3(\lambda)\theta_0^4\right\}\left(\frac{\delta}{t}\right)^3+\frac{1}{\alpha}\left\{f_4(\lambda)+f_5(\lambda)\theta_0^2\right\}\left(\frac{\delta}{t}\right)^2$$
$$+f_6(\lambda)\left(\frac{\delta}{t}\right)+\frac{1}{\alpha^2}\left\{f_7(\lambda)+f_8(\lambda)\theta_0^2\right\}\left(\frac{\delta}{t}\right), \tag{20}$$

where

$$\alpha=a\theta_0^2/t. \tag{21}$$

4. Discussions of Analytical Results

The partial cylindrical shell or the curved plate has frequently a practical importance as a segment in the reinforced structure where λ is not so large, so the numerical examples for the cases of $\lambda=1/1$ and $1/3$ will be given here. Taking ν equal to $1/3$, $f_1(\lambda), f_2(\lambda), \cdots, f_8(\lambda)$ are shown in Table 1.

Table 1

$f(\lambda)$ / λ	$f_1(\lambda)$	$f_2(\lambda)$	$f_3(\lambda)$	$f_4(\lambda)$	$f_5(\lambda)$	$f_6(\lambda)$	$f_7(\lambda)$	$f_8(\lambda)$
1/1	2.5431	0.4116	−0.2892	−1.7357	−0.1876	0.4394	3.4388	0.2508
1/3	4.7031	5.1493	−2.4764	−2.8586	−2.4771	0.4796	2.4358	0.2148

The relations between the pressure and the maximum deflection are shown in Fig. 5 and Fig. 6 with the parameter of α according to Eq. (20). For the case of $\lambda=1/1$ (Fig. 5), if θ_0^2 is small the pressure–deflection curves show little difference

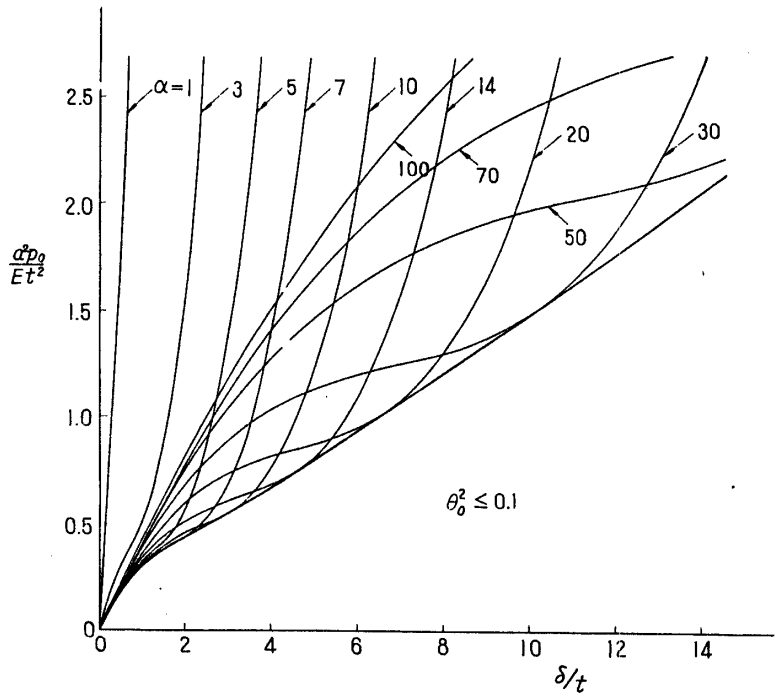

Figure 5. The pressure–deflection curves, $\lambda=1/1$.

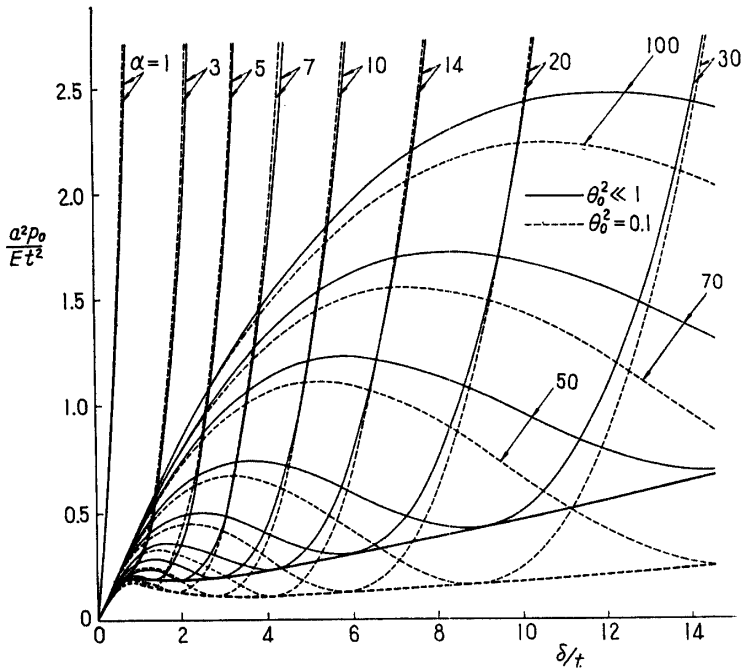

FIGURE 6. The pressure-deflection curves, $\lambda=1/3$.

among them. On the other hand, for the case of $\lambda=1/3$ (Fig. 6), the curves become to vary a little with the value of θ_0^2, because the coefficients of θ_0^2 and θ_0^4 in Eq. (20) $[f_2(\lambda), f_3(\lambda)$ and $f_5(\lambda)]$ take larger values as seen in Table 1. When the value of θ_0^2 is specified as shown in Fig. 6, each curve with the parameter of α means the one for the specific value of a/t, since α is equal to $a\theta_0^2/t$.

For the case of small value of α, the pressure increases monotonously with an increase of deflection; however, as α becomes larger, the pressure–deflection curves become to present the maximum and minimum points, in other words, the "Durchschlag" (snapping) phenomenon becomes to take place. The maximum pressure (M_1) and the minimum pressure (N_1) in the equilibrium curve [Fig. 7(a)] are

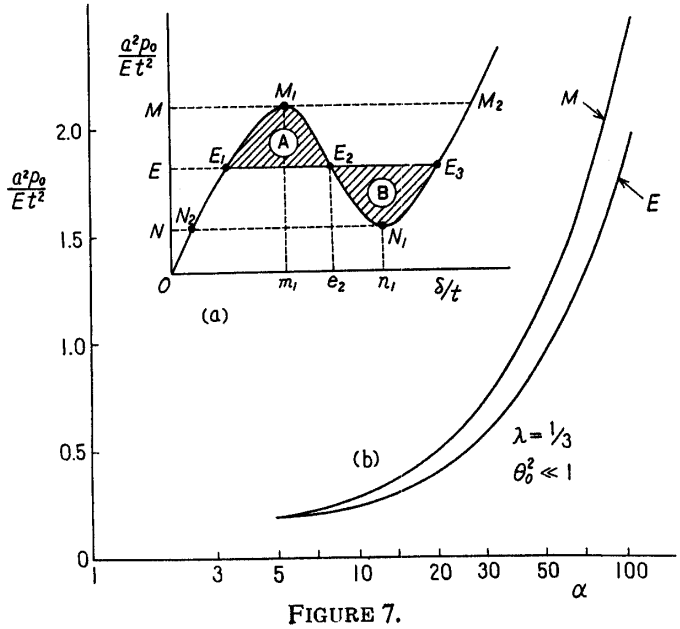

FIGURE 7.

obtained from the condition of $d(a^2p_0/Et^2)/d(\delta/t)=0$ in Eq. (20) in a form as

$$\left(\frac{\delta}{t}\right)_{\substack{m_1\\n_1}}=\frac{C\pm\sqrt{D}}{B}. \tag{22}$$

From which, it can easily be seen that $D>0$ or

$$\alpha^2>\frac{3\{f_1(\lambda)+f_2(\lambda)\theta_0^2+f_3(\lambda)\theta_0^4\}\{f_7(\lambda)+f_8(\lambda)\theta_0^2\}}{\{f_4(\lambda)+f_5(\lambda)\theta_0^2\}^2-3\{f_1(\lambda)+f_2(\lambda)\theta_0^2+f_3(\lambda)\theta_0^4\}\cdot f_6(\lambda)}\equiv\alpha_d^2 \tag{23}$$

is the condition for the "Durchschlag" phenomenon to take place, and for the region of $\alpha^2<\alpha_d^2$ the pressure increases monotonously with the deflection. For the case of $\lambda=1/1$, if θ_0^2 is small in the order of $\theta_0^2\leqq0.1$ the "Durchschlag" buckling does not occur, but for the case of $\lambda=1/3$ the unstable zones exist if $\alpha>4.9$ ($\theta_0^2\ll1$) and $\alpha>4.2$ ($\theta_0^2=0.1$) From the above analytical results, it is found that "Durchschlag" buckling phenomenon may take place easily, if the axial length of cylindrical shell is longer (smaller λ), the center angle of the curved surface is larger (larger θ_0^2) and the shell is thinner with the larger radius of curvature (larger a/t).

Next, let us consider about the buckling pressures. If it is assumed that there exists no external disturbance during the pressure loading and no imperfection in the cylindrical shell, the deflection will increase with an increrse of the pressure along $ON_2E_1M_1$ in Fig. 7(a), and the shell will be forced to buckle at the maximum pressure M_1. In this buckling process, the pressure will usually drop depending on the elastic rigidity of loading machine, but if the pressure is applied by the dead load the deflection increases suddenly from M_1 to M_2 under constant pressure. So the pressure at the point M_1 is considered as "the upper buckling pressure". The values of the upper buckling pressure $(a^2p_0/Et^2)_M$ for the case of $\lambda=1/3$ and $\theta_0^2\ll1$ are plotted against α in Fig. 7(b), and they increase monotonously with α.

If there are some imperfections in the loading machine and the shell specimen, the buckling pressure will be much lower. But, if not so, it should be considered necessary to jump over the energy barrier to buckle under the pressure lower than the upper buckling pressure. If the above imperfections are assumed to be equivalent to the energy barrier, it seems reasonable to consider the pressure having the equal value of total potential energies at the equilibrium positions before and after buckling under a constant external pressure and to define it as the lower possible buckling pressure as proposed by Tsien [*6*]. Such an analytical consideration was described before in detail in the paper for the case of the spherical shell [*3*], so it is shown briefly here. The non-dimensional total potential energy Π' is expressed as

$$\Pi'=\Pi_i'\text{ (strain energy)}+\Pi_a'\text{ (potential energy of external force)}$$
$$\propto\int_0^{\frac{\delta}{t}}\frac{a^2p_0}{Et^2}d\left(\frac{\delta}{t}\right)-\frac{a^2p_0}{Et^2}\int_0^{\frac{\delta}{t}}d\left(\frac{\delta}{t}\right). \tag{24}$$

Paying our attention to the fact that the pressure–deflection curve is presented by a cubic algebraic equation and the curve is antisymmetrical with respect to the mid point E_2 in M_1N_1, and the area Ⓐ which denotes the energy barrier to be jumped over is equal to the area Ⓑ in Fig. 7(a), then it can be found from Eq. (24)

that the total potential energies at both points of E_1 and E_3 are equal in the buckling process $E_1 \rightarrow E_2 \rightarrow E_3$ under the constant external pressure $(a^2p_0/Et^2)_E$. In this case, the possibilities of occurrence of buckling from E_1 to E_3 and of its reverse course are equal and so the pressure at the point E can be designated as the actually probable buckling pressure or the so-called "the lower buckling load". The values of $(a^2p_0/Et^2)_E$ for the case of $\lambda=1/3$ and $\theta_0^2 \ll 1$ are shown against α in Fig. 7(b). The lower buckling pressures also increase as α is increased. It is worth noting that there exists no minimum value for $(a^2p_0/Et^2)_E$ against α as seen in this curve which is different from the case for the spherical shell [3].

The non-dimensional values of (a^2p_0/Et^2) for these buckling pressures defined above increase with α as seen in Fig. 7; however, if the ordinate is converted to (p_0/E), the values of buckling pressure themselves decrease with an increase of a/t, because if θ_0^2 is considered to be constant, the increase of α corresponds to the increase of a/t. This situation can be seen in Fig. 8 for the case of $\theta_0^2=0.1$. On the

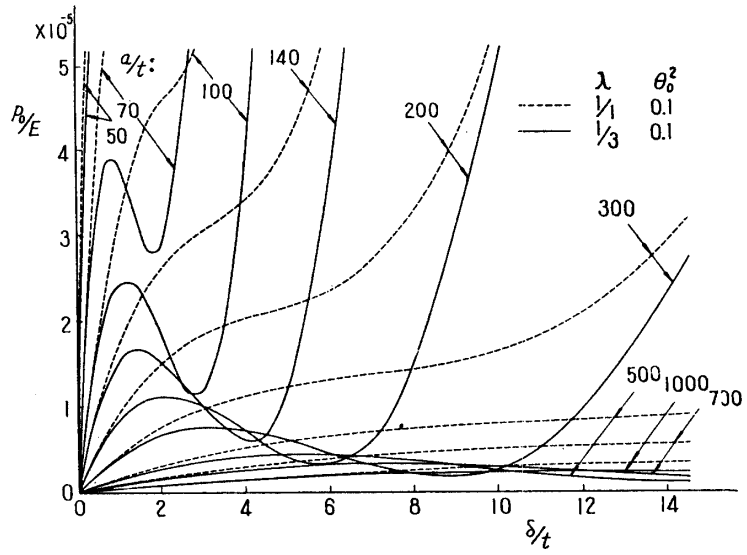

FIGURE 8. The pressure-deflection curves, $\theta_0^2=0.1$.

other hand, if a/t is considered to be constant, the critical buckling values increase much more with θ_0^2 because of the increase of $\alpha=a\theta_0^2/t$, although there is the negative fact that the buckling pressures decrease a little with an increase of θ_0^2 resulting from the more rigorous analysis considering the terms concerning θ_0^2 and θ_0^4 in Eq. (20) as seen in Fig. 6.

In estimating the order of magnitudes on the curvatures of the median surface, the changes of curvature and the strains at the start of this analysis, we imposed no restriction on the magnitude of θ_0. In consequence, this analysis can be applied to the case of larger θ_0 in principle, but the larger θ_0 becomes, the larger the deflection δ may become, which is not consistent with the assumptions that δ/y_0 and δ/l are the infinitesimal quantities of the first order. For this reason, in the case where θ_0 is larger, the analytical results in the region with larger deflection are some doubtful about its accuracy and so the terms of higher order on the displacement must be taken into account in the analysis as shown in the case for the

spherical shell [4].

The mode of pressure distribution over the surface enters only in the term of $\iint pw\,dx\,dy$ in Eq. (18), so the effect of pressure distribution on the buckling pressure may be expressed by a constant correction factor under an assumed deflection, for example, if p is assumed to be constant over the surface, that is $p=p_0$ instead of $p=p_0(1-y'^2)$ as in Eq. (19), then the analytical results may be used only with a slight correction of multiplying the left hand side of Eq. (20) by 1.167. In other words, the diagrams of Figs. 5, 6 and 8 with ordinates multiplied by a constant $=0.857$ can be used as they stand for the case of $p=p_0$ without an appreciable error.

Futhermore, the deflection w was assumed as a first approximation as usually done in non-linear problems in elasticity and only a symmetrical shape was considered. However, the deflection mode has so great effect on the buckling pressure that we must be careful in choosing the assumed deflection. The further investigation of the effect of the deflection mode on the buckling value has been carried out which will be published later in detail.

In the case for the cylindrical shell, it was so difficult to present the analytical expressions comprehensively with the satisfactory accuracy because of more parameters involved that only a case with a special boundary conditions was shown as an example. But, the cases with other boundary conditions can be analyzed with the same process as described in this paper by using any w which satisfies the boundary conditions.

Department of Structures,
Aeronautical Research Institute,
University of Tokyo, Tokyo.
April 20, 1960.

References

[1] Yoshimura, Y. and Uemura, M.: The Buckling of Spherical Shells due to External Pressure, Inst. Sci. Tech., Univ. of Tokyo, Report **3** (1949) 316.

[2] Uemura, M. and Yoshimura, Y.: The Buckling of Spherical Shells by External Pressure (2nd Report Especially on the Lower Buckling Load and Energy Barrier), Inst. Sci. Tech., Univ. of Tokyo, Report **6** (1952) 367.

[3] Uemura, M.: The Buckling of Spherical Shells by External Pressure (3rd Report Buckling Mechanism of Spherical Shell Segments), Jour. Japan Soc. Aero. Engg., **2** (1954) 113.

[4] Uemura, M.: The Buckling of Spherical Shells by External Pressure (4th Report), Jour. Japan Soc. Aero. Engg., **4** (1956) 273.

[5] Yoshimura, Y.: Theory of Thin Shells with Finite Deformation, Inst. Sci. Tech., Univ. of Tokyo, Report **2** (1948) 167, 3 (1949) 19.

[6] Tsien, H. S.: A Theory for the Buckling of Thin Shells, Jour. Aero. Sci., 9 (1942) 373.